

# Lensing simulations by Taylor expansion – not so inefficient after all

Sigurd K. Naess\* and Thibaut Louis

*Sub-department of Astrophysics, University of Oxford, Keble Road, Oxford, OX1 3RH, UK*

Cosmic Microwave Background lensing simulation by Taylor expansion has long been considered impractical due to slow convergence, but a recent flat-sky implementation shows that a simple trick eliminates this problem, making Taylor lensing a fast and simple lensing algorithm for the flat sky. Here we generalize the method to the full sky, and study its convergence and performance relative to a commonly used numerical code, Lenspix, with extensive benchmarks of both. Compared to the flat sky case, the method takes a speed hit due to the slow speed of spherical harmonic transforms compared to fast Fourier transforms, resulting in speeds of  $\frac{1}{3}$  to  $\frac{2}{3}$  of Lenspix for similar accuracy.

## I. INTRODUCTION

On its way from the surface of last scattering to us, the Cosmic Microwave Background radiation (CMB) is weakly lensed by the gravitational potential of the intervening large scale structure [1]. This introduces a non-linear distortion that was first detected as a correlation between the CMB and large scale structure using WMAP data Smith *et al.* [2], Hirata *et al.* [3], and has since been measured directly in the CMB at progressively increasing sensitivity by ACT [4, 5], SPT [6–8] and Planck [9].

As CMB lensing measurements improve, they have the potential to be some of the cleanest probes of the total matter distribution in the universe, especially when coupled with galaxy surveys. This will make them powerful probes for neutrino masses [10] and the nature of dark matter and dark energy [11].

On the scales relevant for CMB observations, this lensing is weak enough to be modeled as a simple displacement in accordance with the Born approximation [1],

$$T'(\vec{x}) = T(\vec{x} + \vec{\alpha}) \quad (1)$$

$$\vec{P}'(\vec{x}) = R\vec{P}(\vec{x} + \vec{\alpha}), \quad (2)$$

where  $T'$  ( $T$ ) and  $\vec{P}'$  ( $\vec{P}$ ) are the lensed (unlensed) temperature and polarization fields;  $\vec{\alpha} = \nabla\phi$  is the displacement field, with  $\phi$  being the lensing potential; and  $R$  is a polarization rotation matrix which is very nearly unity<sup>1</sup> [12].

Conceptually, constructing a lensed map is as simple as reading off values from the unlensed map at the appropriate positions, but in practice this is complicated by the fact that computers work with discretely sampled maps. Hence, the value of the map is only known at some points on the sphere, which will in general not include the displaced position  $\vec{x} + \vec{\alpha}$ . The problem of lensing a CMB map hence becomes one of *interpolation*.

Several methods for performing this interpolation have been explored in the literature, including:

1. Nearest neighbor remapping, i.e. truncating the offset position to the nearest pixel, and using that as the offset value. This leads to severe pixelization errors, but for CMB simulations these can be mitigated by generating the map at much higher resolution than needed, remapping at this resolution, and then downgrading in the end [12, 13]. However working with higher than necessary resolution maps comes with a large performance and memory overhead.
2. Taylor expansion in terms of the displacement  $\vec{\alpha}$ :

$$T(\vec{x} + \vec{\alpha}) = \sum_{n,j \leq n} \frac{\alpha_{\theta}^j \alpha_{\phi}^{n-j}}{j!(n-j)!} \left[ \partial_{\theta}^j \partial_{\phi}^{n-j} T \right] (\vec{x}). \quad (3)$$

While conceptually simple, this algorithm scales with the expansion order  $n$  as  $\mathcal{O}(n^2)$ , which coupled with its slow convergence makes it inefficient in practice [12, 14].

3. Direct evaluation of spherical harmonics at the offset locations, i.e.  $T(\vec{x} + \vec{\alpha}) = \sum_{lm} T_{lm} Y_{lm}(\vec{x} + \vec{\alpha})$ , where  $T_{lm}$  are the spherical harmonic coefficients of the unlensed map. Sadly, spherical harmonics transformations (SHTs) are very expensive for unevenly spaced pixels [12], though the method can be sped up by recasting it as a non-equidistant fast Fourier transform on the torus [15].
4. Constrained realizations based on the neighboring pixels and the known statistical properties of the signal. This is in theory exact, but in practice simplifying approximations of the signal correlations are necessary for computational tractability [16].
5. The use of interpolation-friendly pixelization schemes, such as ECP. This over-pixelizes the sphere compared to HEALPix, but the regular grid makes it easy to implement many interpolation schemes from standard image processing, such as bi-cubic interpolation. It can also be used to speed up some of the previously mentioned methods. This is the technique used by the popular [2, 7, 9] Lenspix algorithm [12].

\* Sigurd.Naess@astro.ox.ac.uk

<sup>1</sup> This rotation has two contributions. Firstly, the lensing itself introduces a vanishingly small rotation of the polarization angle, which is sometimes called “gravitational Faraday-rotation”. Secondly, parallel transport on the sphere results in a much larger but still small rotation which is most significant near the poles.

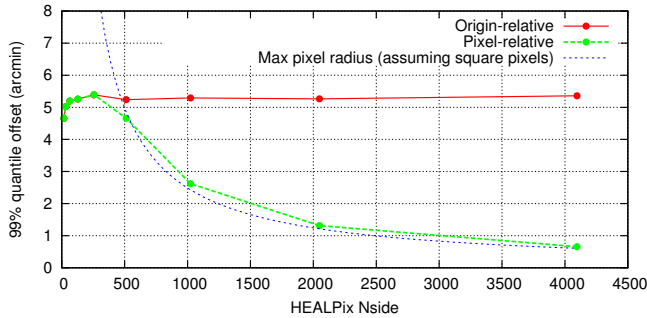


Figure 1. Comparison of the interpolation distance for plain Taylor expansion (red) versus expansion relative to the nearest pixel center (green). The 99% quantile of the lensing deflection is 5.3' in our simulations. For  $N_{\text{side}} > 512$ , the pixel radius (blue) is smaller than this, making pixel-relative expansion increasingly efficient at higher resolution, as a smaller expansion parameter means we converge earlier.

In a recent paper, Louis *et al.* [17] showed that a trivial modification of the Taylor expansion method cures it of its slow convergence, and demonstrated its excellent accuracy and speed for flat-sky lensing simulations.

In general, the Taylor expansion of a function  $f(x)$  around a point  $x_0$  becomes less accurate as the distance from  $x_0$  grows, and conversely, the expansion can be truncated earlier if one can expand around a point close to where one wishes to evaluate the function.

The Taylor expansion used in the literature [9, 12, 18] expands  $T(\vec{x} + \vec{\alpha})$  around the point  $\vec{\alpha} = 0$ , and the reason for the slow convergence is that  $\vec{\alpha}$  can be relatively large compared to the scales involved in the map. A better choice is to expand around the closest pixel center  $\vec{\alpha}_0$ , which is already exactly available, resulting in the following expansion:

$$\begin{aligned}
 T'(\vec{x}) &= T(\vec{x} + \vec{\alpha}_0 + \Delta\vec{\alpha}) \\
 &= \sum_{n,j \leq n} \frac{\Delta\alpha_\theta^j \Delta\alpha_\phi^{n-j}}{j!(n-j)!} \left[ \partial_\theta^j \partial_\phi^{n-j} T \right] (\vec{x} + \vec{\alpha}_0). \quad (4)
 \end{aligned}$$

At higher resolutions, this results in an expansion in terms of a much smaller parameter compared to the standard expansion around the undisplaced location, as shown in figure 1.

For the flat sky, this, combined with fast Fourier transforms (FFTs) for computing the derivatives, results in fast lensed simulations at 0.5 arcminute that are accurate at all relevant scales by order 2 in the expansion, with no pixel upscaling needed [17].

However, this does not necessarily generalize to the full sky. Firstly, the resolutions relevant for full-sky simulations are much lower. This means that more important parts of the unlensed power spectra will be truncated. And secondly, SHTs are much slower than FFTs

<sup>2</sup>, so computing the derivatives in harmonic space is much more expensive here than on the flat sky.

The purpose of this paper is to empirically test how important these issues are in practice by determining the performance of nearest neighbor Taylor interpolation for full-sky CMB simulations.

## II. IMPLEMENTATION

### A. Preparing the input

The main interpolation step of the algorithm needs a map to lens and a mapping from lensed to unlensed coordinates that describes the lensing field. If these are already present from other sources, no further preparation is needed, and this step can be skipped.

But often one needs to generate lensed maps from scratch, such as for the accuracy tests in the next section. For this, we simulated HEALPix-pixelated [19] CMB maps (using `healpy.synfast`) and corresponding displacements  $\nabla\phi$  (using `healpy.synalm` and `healpy.alm2map_der1`) with no pixel window. These were based on theoretical unlensed spectra from CAMB, for a  $\Lambda$ CDM cosmological model. For the gradient calculation we used  $\ell_{\text{max}}^{\nabla\phi} = \min(8N_{\text{side}}, 10000)$ . This value is much higher than what is normally necessary, but is important because the gradient map acts like a high-pass filter and is very sensitive to small scales. This high  $\ell_{\text{max}}^{\nabla\phi}$  comes at a cost in performance, but it is usually subdominant compared to the other steps, and we did not attempt to fine-tune  $\ell_{\text{max}}^{\nabla\phi}$  for optimal performance.

The offset positions  $\vec{x}' = \vec{x} + \nabla\phi$  were then computed both via parallel transport using equations (A15-A16) in [12] and by the naive method of simply adding the coordinates, which we found to make no practical difference (see fig. 7).

### B. Interpolating

With an unlensed map  $m$  and a position map  $\vec{x}'$  in hand, we can now calculate the set of nearest pixels  $\{p\}$  using `healpy.ang2pix`, their center locations  $\vec{x}'_0$  via `healpy.pix2ang`, and the subpixel offset  $\Delta\vec{\alpha} = \vec{x}' - \vec{x}'_0$ .<sup>3</sup> We then Taylor-expand each component  $s \in \{T, Q, U\}$  of the map  $m$  independently to estimate the value  $T'(\vec{x})$

<sup>2</sup> Currently practical SHTs scale as  $(O)N_{\text{pix}}^{\frac{3}{2}}$ , compared to  $(O)N_{\text{pix}} \log(N_{\text{pix}})$  for FFTs, and additionally the prefactor is much larger for SHTs.

<sup>3</sup> As `healpy.alm2map_der1` actually returns  $\left(\frac{\partial m}{\partial \theta}, \frac{\partial m}{\sin \theta \partial \phi}\right)$ , the expansion we performed in practice was in terms of  $(\Delta\alpha_\theta, \sin \theta \Delta\alpha_\phi)$  to avoid needing to rescale all the derivatives.

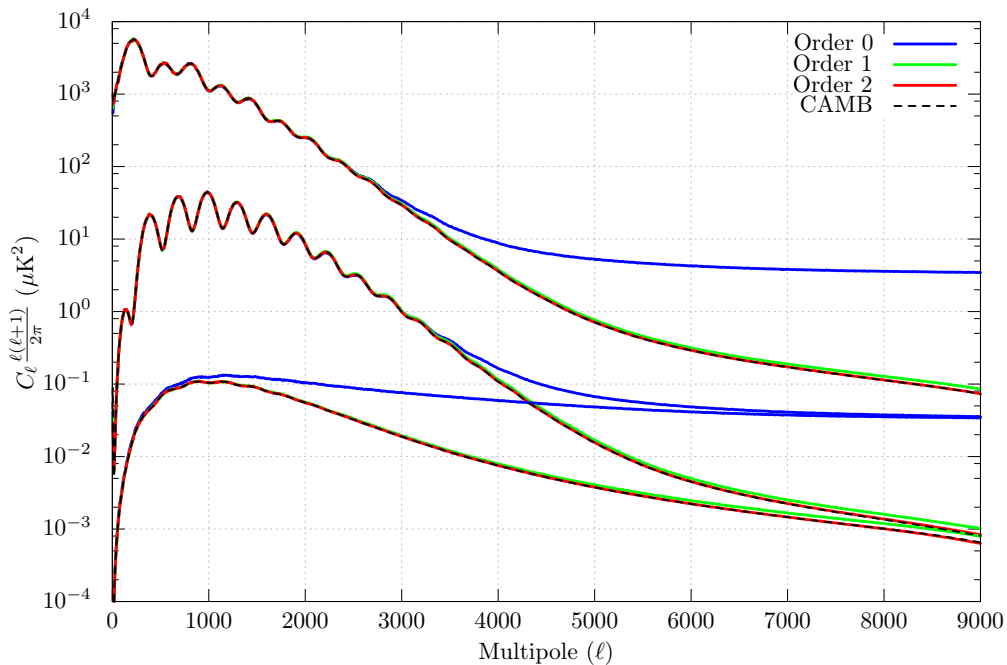


Figure 2. Illustration of the convergence of the pixel-relative Taylor expansion at  $N_{\text{side}} = 4096$  for the TT (top), EE (middle) and BB (bottom) spectra. The blue, green and red curves corresponds to stopping the expansion at order 0, 1 and 2 respectively. The black curve is the theoretical result from CAMB. On this absolute scale, the order 2 curve is indistinguishable from theory. See figure 3 for a more quantitative treatment of the convergence.

and  $P'(\vec{x})$ :

$$s'(\vec{x}) = \sum_{n,j \leq n} \frac{\Delta \alpha_\theta^j \Delta \alpha_\phi^{n-j}}{j!(n-j)!} \left[ \partial_\theta^j \partial_\phi^{n-j} s \right] (\vec{x}'_0), \quad (5)$$

where the higher derivatives were computed by repeated applications of `healpy.map2alm`<sup>4</sup> and `healpy.alm2map_der1`.

Using the fact that `healpy.alm2map_der1` returns two derivatives at the same time, only  $\lfloor \frac{n}{2} \rfloor + 1$  forward and backward SHTs are needed for each order  $n > 0$  in the expansion, for a total of  $N + \lfloor \frac{N}{2} \rfloor$  ( $\lfloor \frac{N+1}{2} \rfloor + 1$ ) two-way SHTs when stopping at order  $N$ .

Finally, the lensed polarization map can be corrected for the effect of rotation (i.e. the matrix  $R$  in eq. 2) due to parallel transport using equations (A17-A18) in [12], though we found this to have no appreciable effect on the power spectrum at any any of the scales we tested.

A small python library implementing this algorithm, called `Taylens`, is available at [20].

### III. RESULTS

#### A. Accuracy and convergence

We performed two sets of tests of the algorithm. In the first, we systematically investigated accuracy and convergence by generating a large number of simulations (256 for all but the highest resolution) for each  $N_{\text{side}} \in \{512, 1024, 2048, 4096\}$  and for each expansion order from 0 to 4. We here used the HEALPix default  $\ell_{\text{max}} = 3N_{\text{side}}$  as the accuracy of the calculation of the derivatives in the expansion (but not when generating the deflected positions). The power spectra of the resulting maps were computed using `healpy.anafast`, and were then compared with the result of a high-accuracy CAMB simulation.

The result can be seen in figures 2 and 3. As others have observed, order 0 (naive nearest neighbor lookup) performs very poorly, and fails to produce the correct BB power at any scale even at the highest resolutions. But from order 2 the accuracy quickly improves, and the series is close to converged by order 4, where it is typically accurate at the 0.5% level up to  $1.5N_{\text{side}} \lesssim \ell \lesssim 2N_{\text{side}}$ . The series converges faster at higher resolutions, and at  $N_{\text{side}} = 4096$  it is almost fully converged by order 2, where it is accurate up to  $\ell \sim 6000$ , which is close to the accuracy limit of CAMB.

<sup>4</sup> We found that using `iter=0` led to no appreciable loss in accuracy while giving a great increase in speed compared to the default `iter=3`.

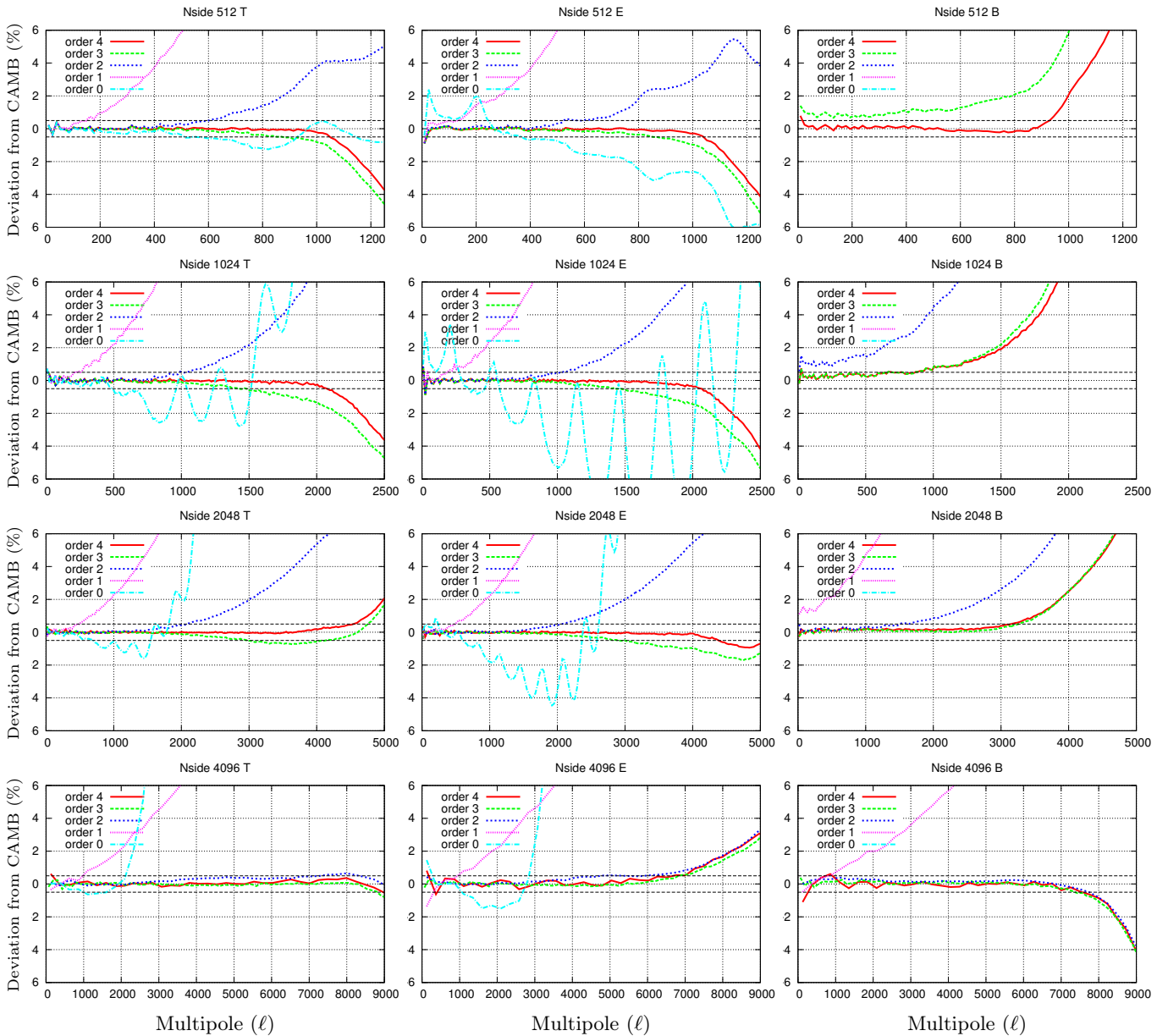


Figure 3. The relative error (in %) of Taylor lensing in terms of its output power spectra compared to the theoretical CAMB lensed spectra as a function of multipole. The three columns are TT, EE and BB, while the four rows are simulation  $N_{\text{side}}$  of 512, 1024, 2048 and 4096 respectively. Each panel shows the error for truncating the Taylor expansion at orders 0 to 4 inclusive. Typically all spectra are accurate to less than 0.5% up to a multipole of  $1.5N_{\text{side}}$  to  $2N_{\text{side}}$  at order 4. The curves are averages over 256 simulations (with the exception of  $N_{\text{side}} = 4096$ , where fewer were used due to high cost).

## B. Benchmarks

In the second test, we investigated the performance of the algorithm, and compared it with Lenspix, the most popular lensing simulator at the time of writing. Lenspix is an example of a local interpolation scheme, and estimates the value of the CMB at the lensing-displaced positions by using bi-cubic interpolation after repixlizing the sky in Equi-Cylindrical coordinates. Both Lenspix and our HEALPix-based implementation

of Taylor lensing (Taylens) have 3 parameters that affect accuracy and speed: The resolution  $N_{\text{side}}$ , the highest multipole  $\ell_{\text{max}}$  used in SHTs, and the interpolation order. In order to test each algorithm at their best, we tested every combination of  $N_{\text{side}} \in \{256, 512, 1024, 2048, 4096\}$ ,  $\ell_{\text{max}} \in \{N_{\text{side}}, \frac{3}{2}N_{\text{side}}, 2N_{\text{side}}, \frac{5}{2}N_{\text{side}}, 3N_{\text{side}}\}$  and order  $\in \{0, 1, 2, 3, 4\}$  for Taylens and order  $\in \{1.0, 1.5, 2.0, 2.5, 3.0\}$  for Lenspix, for a total of 150 combinations for each. Due to computational constraints, only 1 simulation was performed for each of these.

The benchmarks were performed on 8 core 2.53 GHz Xenon E5540 nodes on the SciNet cluster. All reported times are total CPU times added up across all 8 cores unless noted otherwise.

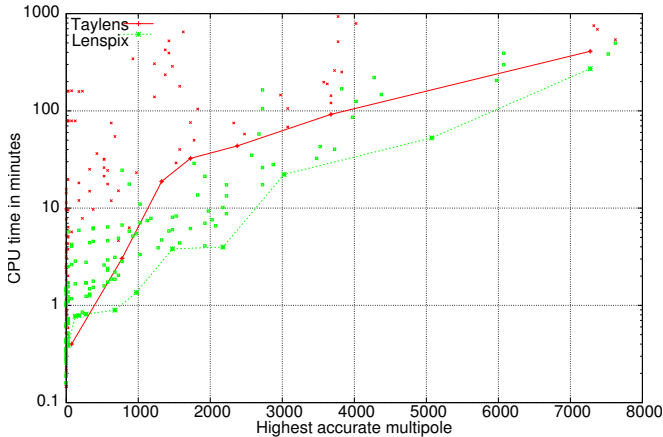


Figure 4. Comparison of the performance of a python implementation of the Taylor lensing algorithm described in this paper (Taylens, red, crosses/solid line) with that of the popular Lenspix (green, boxes, dashed line). Only the interpolation step (which is where they differ) is included in the times. To find the optimal parameters for each of these, parameters were systematically varied, resulting in the set of small red and green points. The lower envelopes of these sets of points is an estimate of the optimal performance, and are shown with lines. The horizontal axis indicates the maximum multipole for which TT, EE and BB are all within 0.5% of the theoretical prediction CAMB, while the vertical axis is the total CPU time in minutes. Taylens is slower than Lenspix by a factor of  $\sim 3$  for most relevant scales.

The resulting accuracy vs. CPU time is plotted in figure 4, and the most efficient combinations found are summarized in table I. The highest accurate multipole  $\ell^*$  is defined here as the center of the last  $\Delta\ell = 50$  bin of each of the spectra that is not significantly ( $< 4\sigma$ ) above the 0.5% accuracy limit.

In general, Taylor lensing is slower than Lenspix by a factor of  $\sim 3$  for most relevant accuracies, but towards the very highest accuracies this factor decreases to 1.5. Compared to the flat-sky case, Taylor lensing with harmonic derivatives is hampered by the  $\mathcal{O}(N_{\text{pix}}^{\frac{3}{2}})$  scaling of the SHT, compared to the  $\mathcal{O}(N_{\text{pix}} \log N_{\text{pix}})$  scaling of the flat-sky FFT. However, due to the quicker convergence at higher resolution, the effective scaling is significantly better than the naive estimate of  $\mathcal{O}(\ell^3)$  one would expect based on SHT scaling, and for the parameter range probed here, it seems to be closer to  $\mathcal{O}(\ell^2)$ .

<sup>5</sup> The threshold of  $4\sigma$  was chosen to be high enough that it would be unlikely to be reached due to a random fluctuation.  $\sigma$  here refers to the uncertainty of the measured mean in each  $\Delta\ell = 50$  bin.

As an example, creating a lensed map accurate up to a multipole of 3000 took 68 minutes (8.5 minutes on 8 cores) using Taylens, and 22 minutes (2.8 minutes on 8 cores) using Lenspix <sup>6</sup>.

## IV. CONCLUSION

Lensing simulation by nearest neighbor-relative Taylor expansion is a fast, simple and accurate lensing method on the flat sky, but for the full sky we find it to be hampered by the poor scaling of spherical harmonic transforms compared to fast Fourier transforms. Nevertheless, our extensive benchmarks show that it performs quite well on the full sky, reaching  $\frac{1}{3}$  to  $\frac{2}{3}$  of the speed of the highly optimized Lenspix code, while being very simple to implement <sup>7</sup>.

The dependence on slow SHTs can be broken by switching to a local pixel-space estimator for the derivative, though this is somewhat cumbersome on the curved sky, and may be less accurate than the harmonic derivatives used here. A better pixel-local approach would probably be the constrained realization lensing used in FLINTS [16].

Alternatively, switching to ECP pixelization would make FFTs available, for a potentially large speed-up (though at the cost of extra projection operations if one still wishes the output to be in standard HEALPix coordinates).

## ACKNOWLEDGMENTS

The authors would like to thank Johannes Noller and Jo Dunkley for useful discussion. Computations were performed on the gpc supercomputer at the SciNet HPC Consortium. SciNet is funded by: the Canada Foundation for Innovation under the auspices of Compute Canada; the Government of Ontario; Ontario Research Fund - Research Excellence; and the University of Toronto. SN and TL are supported by ERC grant 259505.

## Appendix: Performance details

Table I shows the most cost-efficient parameters found during the brute force parameter benchmarks, defined as the parameters making up the lower-time envelope of the accuracy vs. time distribution.  $N_{\text{side}} \sim \frac{2}{3}\ell^*$ ,  $\ell_{\text{max}} \sim$

<sup>6</sup> Taylens indirectly benefits from HEALPix’s OpenMP parallelization for lensing single maps, and also uses minimal MPI for lensing several independent maps in parallel.

<sup>7</sup> Our demonstration implementation consists of 253 lines of Python, including comments, I/O and user interface, and depends only on healpy and numpy.



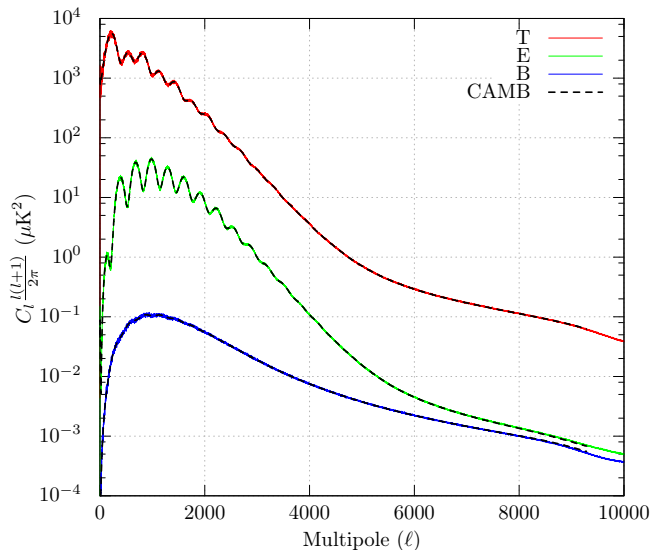


Figure 5. Comparison of the  $N_{\text{side}} = 4096$  order 3 Taylens spectra (colored curves) with the CAMB lensed spectra (dashed black curves).

$\ell^* + 2000$  seems to be a good default choice for both Taylens and Lenspix.

As can be seen from figure 4, the impact of parameter choice is large – roughly twice as large as the performance difference between Taylens and Lenspix for the parameters we explored.

The lensed spectra from Taylens and CAMB are compared on an absolute scale in figure 5. While the accuracy information in this graph is the same as (but harder to see than) figure 6, this view shows the large dynamic range over which the simulations are accurate, which is comparable to that of a 32-bit floating point number.

At the higher accuracies tested in the benchmarks, both Taylens and Lenspix exhibit very similar patterns of deviation from CAMB (see figure 6), and both fail to improve further when higher interpolation orders or  $\ell_{\text{max}}$  are used. This points to the error not being in the interpolation method, but in either the input unlensed power spectrum from CAMB (which is truncated at  $\ell = 10000$  and not very accurate for  $\ell > 6000$ ), or the lensed CAMB power spectrum that we are comparing with. If so, it is possible that the accuracy of both Taylens and Lenspix extends beyond  $\ell = 8000 - 9000$  with these settings.

- 
- [1] A. Lewis and A. Challinor, Phys.Rep. **429**, 1 (2006), arXiv:astro-ph/0601594.
- [2] K. M. Smith, O. Zahn, and O. Doré, Phys. Rev. D **76**, 043510 (2007), arXiv:0705.3980.
- [3] C. M. Hirata, S. Ho, N. Padmanabhan, U. Seljak, and N. A. Bahcall, Phys. Rev. D **78**, 043520 (2008), arXiv:0801.0644.
- [4] S. Das, B. D. Sherwin, P. Aguirre, J. W. Appel, J. R. Bond, C. S. Carvalho, M. J. Devlin, J. Dunkley, R. Dünner, T. Essinger-Hileman, J. W. Fowler, A. Hajian, M. Halpern, M. Hasselfield, A. D. Hincks, R. Hlozek, K. M. Huffenberger, J. P. Hughes, K. D. Irwin, J. Klein, A. Kosowsky, R. H. Lupton, T. A. Marriage, D. Marsden, F. Menanteau, K. Moodley, M. D. Niemack, M. R. Nolta, L. A. Page, L. Parker, E. D. Reese, B. L. Schmitt, N. Sehgal, J. Sievers, D. N. Spergel, S. T. Staggs, D. S. Swetz, E. R. Switzer, R. Thornton, K. Visnjic, and E. Wollack, Physical Review Letters **107**, 021301 (2011), arXiv:1103.2124 [astro-ph.CO].
- [5] S. Das, T. Louis, M. R. Nolta, G. E. Addison, E. S. Battistelli, *et al.*, (2013), arXiv:1301.1037 [astro-ph.CO].
- [6] R. Keisler, C. L. Reichardt, K. A. Aird, B. A. Benson, L. E. Bleem, J. E. Carlstrom, C. L. Chang, H. M. Cho, T. M. Crawford, A. T. Crites, T. de Haan, M. A. Dobbs, J. Dudley, E. M. George, N. W. Halverson, G. P. Holder, W. L. Holzapfel, S. Hoover, Z. Hou, J. D. Hrubes, M. Joy, L. Knox, A. T. Lee, E. M. Leitch, M. Lueker, D. Luong-Van, J. J. McMahon, J. Mehl, S. S. Meyer, M. Millea, J. J. Mohr, T. E. Montroy, T. Natoli, S. Padin, T. Plagge, C. Pryke, C. L. Reichardt, J. E. Ruhl, J. T. Sayre, K. K. Schaffer, L. Shaw, E. Shirokoff, H. G. Spieler, Z. Staniszewski, A. A. Stark, K. Story, K. Vanderlinde, J. D. Vieira, and R. Williamson, Astrophys. J. **756**, 142 (2012), arXiv:1202.0546 [astro-ph.CO].
- [7] A. van Engelen, R. Keisler, O. Zahn, K. A. Aird, B. A. Benson, L. E. Bleem, J. E. Carlstrom, C. L. Chang, H. M. Cho, T. M. Crawford, A. T. Crites, T. de Haan, M. A. Dobbs, J. Dudley, E. M. George, N. W. Halverson, G. P. Holder, W. L. Holzapfel, S. Hoover, Z. Hou, J. D. Hrubes, M. Joy, L. Knox, A. T. Lee, E. M. Leitch, M. Lueker, D. Luong-Van, J. J. McMahon, J. Mehl, S. S. Meyer, M. Millea, J. J. Mohr, T. E. Montroy, T. Natoli, S. Padin, T. Plagge, C. Pryke, C. L. Reichardt, J. E. Ruhl, J. T. Sayre, K. K. Schaffer, L. Shaw, E. Shirokoff, H. G. Spieler, Z. Staniszewski, A. A. Stark, K. Story, K. Vanderlinde, J. D. Vieira, and R. Williamson, Astrophys. J. **756**, 142 (2012), arXiv:1202.0546 [astro-ph.CO].
- [8] K. T. Story, C. L. Reichardt, Z. Hou, R. Keisler, K. A. Aird, B. A. Benson, L. E. Bleem, J. E. Carlstrom, C. L. Chang, H. Cho, T. M. Crawford, A. T. Crites, T. de Haan, M. A. Dobbs, J. Dudley, B. Follin, E. M. George, N. W. Halverson, G. P. Holder, W. L. Holzapfel, S. Hoover, J. D. Hrubes, M. Joy, L. Knox, A. T. Lee, E. M. Leitch, M. Lueker, D. Luong-Van, J. J. McMahon, J. Mehl, S. S. Meyer, M. Millea, J. J. Mohr, T. E. Montroy, S. Padin, T. Plagge, C. Pryke, J. E. Ruhl, J. T. Sayre, K. K. Schaffer, L. Shaw, E. Shirokoff, H. G.

<sup>8</sup> Lensing accuracy to  $\ell_{TT}^* > 9000$  with  $\ell_{\text{max}} = 6144$  may seem strange, but recall that the SHTs where  $\ell_{\text{max}}$  applies only are used for computing the derivatives in the expansion, and hence do not affect the 0th order term.

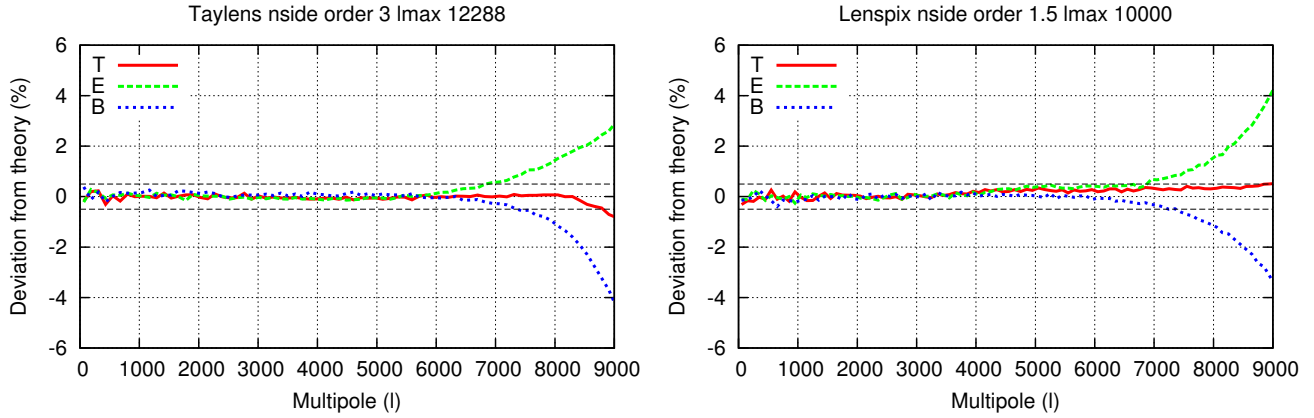


Figure 6. At higher accuracy settings, both Taylens and Lenspix exhibit similar behavior at small scales. This starts happening at  $\ell \sim 7000$ , close to the highest multipole CAMB used in the calculation, and we may hence be seeing inaccuracy of the CAMB spectra rather than Taylens/Lenspix inaccuracy here.

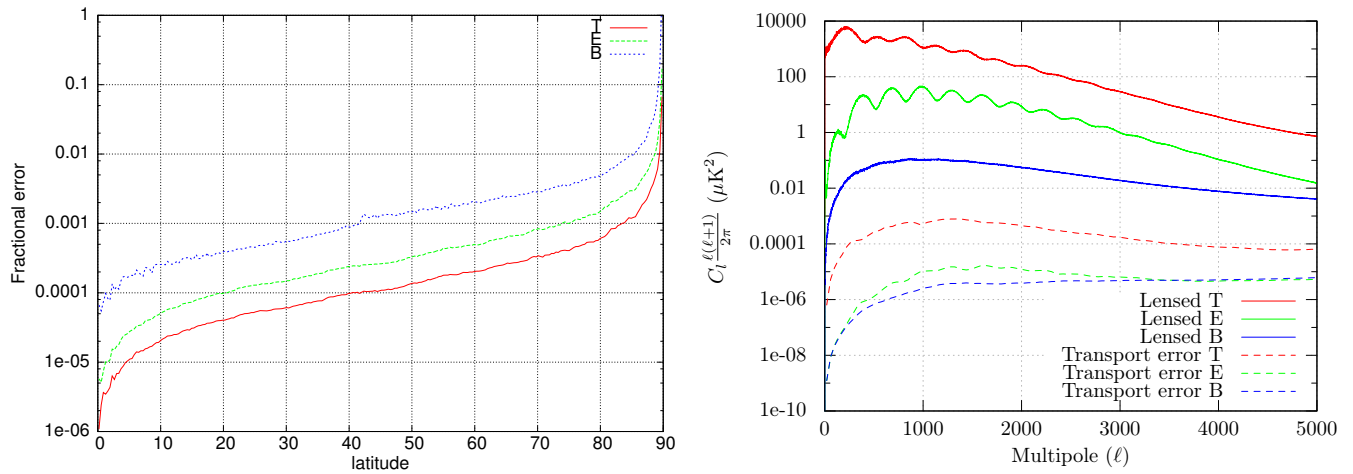


Figure 7. Left panel: The error/signal ratio for the inaccuracy introduced when ignoring rotation from parallel transport as a function of latitude. Calculated as the standard deviation of the error per latitude bin, divided by the signal standard deviation, for each of T, E and B. Excluding the region above  $85^\circ$ , the error is always less than 1%. Right panel: The angular error power spectrum compared with that of the signal, computed for  $N_{\text{side}} = 2048$ . The error is much smaller than the signal at all relevant scales.

- Spieler, Z. Staniszewski, A. A. Stark, A. van Engelen, K. Vanderlinde, J. D. Vieira, R. Williamson, and O. Zahn, ArXiv e-prints (2012), arXiv:1210.7231 [astro-ph.CO].
- [9] Planck Collaboration, P. A. R. Ade, N. Aghanim, C. Armitage-Caplan, M. Arnaud, M. Ashdown, F. Atri-Barandela, J. Aumont, C. Baccigalupi, A. J. Banday, and et al., ArXiv e-prints (2013), arXiv:1303.5077 [astro-ph.CO].
- [10] J. Lesgourgues and S. Pastor, Phys.Rep. **429**, 307 (2006), arXiv:astro-ph/0603494.
- [11] K. M. Smith, W. Hu, and M. Kaplinghat, Phys. Rev. D **74**, 123002 (2006), arXiv:astro-ph/0607315.
- [12] A. Lewis, Phys.Rev. **D71**, 083008 (2005), arXiv:astro-ph/0502469 [astro-ph].
- [13] G. Fabbian and R. Stompor, ArXiv e-prints (2013), arXiv:1303.6550 [astro-ph.CO].
- [14] A. Challinor and A. Lewis, Phys. Rev. D **71**, 103010 (2005), arXiv:astro-ph/0502425.
- [15] S. Basak, S. Prunet, and K. Benabed, ArXiv e-prints (2008), arXiv:0811.1677.
- [16] G. Lavaux and B. D. Wandelt, ApJS **191**, 32 (2010), arXiv:1003.4984 [astro-ph.CO].
- [17] T. Louis, S. Naess, S. Das, J. Dunkley, and B. Sherwin, ArXiv e-prints (2013), arXiv:1306.6692 [astro-ph.CO].
- [18] T. Okamoto and W. Hu, Phys. Rev. D **67**, 083002 (2003), arXiv:astro-ph/0301031.
- [19] K. M. Górski, E. Hivon, A. J. Banday, B. D. Wandelt, F. K. Hansen, M. Reinecke, and M. Bartelmann, Astrophys. J. **622**, 759 (2005), arXiv:astro-ph/0409513.
- [20] S. Naess, “Taylens git repository,” (2013).

<b>Taylens</b>						
$\ell_{TT}^*$	$\ell_{EE}^*$	$\ell_{BB}^*$	$N_{\text{side}}$	$\ell_{\text{max}}$	Order	Time
625	575	75	256	768	2	0.4
1075	1075	775	512	1536	3	3.0
2075	1875	1325	1024	3072	3	18.8
2575	2625	1725	2048	3072	2	32.5
2725	2675	2375	2048	4096	2	43.6
4025	3925	3075	2048	4096	3	68.4
4975	4175	3675	2048	5120	3	92.0
9275	7275	8175	4096	6144 <sup>s</sup>	2	409.9
<b>Lenspix</b>						
$\ell_{TT}^*$	$\ell_{EE}^*$	$\ell_{BB}^*$	$N_{\text{side}}$	$\ell_{\text{max}}$	Order	Time
525	375	25	512	1024	1.0	0.4
1175	1125	975	512	1536	2.0	1.4
2175	1825	1475	1024	2457	1.5	3.8
2175	2225	2175	1024	2560	1.5	4.0
3025	3025	3725	2048	5120	1.5	22.2
5525	5275	5075	2048	6144	2.5	52.8
9275	7275	7625	4096	10000	1.5	271.7

Table I. Table of the settings and results for the Taylens (top) and Lenspix (bottom) lower envelope lines in figure 4. These indicate the highest cost efficiency found in the parameter search. For both Taylens and Lenspix,  $\ell_{\text{max}} \gtrsim \ell_{BB}^* + 2000$  in the range  $1000 \lesssim \ell_{BB}^* \lesssim 4000$  as a rule of thumb. Times are in CPU minutes.